

# Enthalpy Distributions of Arc Jet Flow Based on Measured Laser Induced Fluorescence, Heat Flux and Stagnation Pressure Distributions

Leonard E. Suess,<sup>1</sup> Jim D. Milhoan<sup>2</sup>, Lance Oelke<sup>3</sup>, Dennis Godfrey<sup>4</sup> and Maksim Y. Larin<sup>5</sup>  
*Jacobs Technology, Houston, TX, 77058*

Carl D. Scott<sup>6</sup>  
*LZ Technology, Houston, TX, 77058*

Jay H. Grinstead<sup>7</sup>  
*NASA Ames Research Center, Moffett Field, CA, 94035*

*and*

Steven Del Papa<sup>8</sup>  
*NASA Johnson Space Center, Houston, TX 77058*

**The centerline total enthalpy of arc jet flow is determined using laser induced fluorescence of oxygen and nitrogen atoms. Each component of the energy, kinetic, thermal, and chemical can be determined from LIF measurements. Additionally, enthalpy distributions are inferred from heat flux and pressure probe distribution measurements using an engineering formula. Average enthalpies are determined by integration over the radius of the jet flow, assuming constant mass flux and a mass flux distribution estimated from computational fluid dynamics calculations at similar arc jet conditions. The trends show favorable agreement, but there is an uncertainty that relates to the multiple individual measurements and assumptions inherent in LIF measurements.**

## I. Introduction

One of the objectives of determining the performance of thermal protection materials during entry into the atmosphere is simulating the conditions encountered, including the pressure, heat flux, and enthalpy. Arc jet facilities have been used for testing thermal protection materials and evaluating their performance. Obtaining two of these three parameters has been fairly achievable, but not necessarily all three at one time. Engineers have had to settle with simulating the two parameters that would best apply to the characteristics of the material tested. Usually that is the heat flux, but often the material can chemically react with the environment, so simulating the chemical composition of the flow is needed. The composition of the flow depends largely on the enthalpy. However, the enthalpy is not readily measurable. Estimates of the enthalpy have been made using various techniques in the past, such as the sonic throat technique and the energy balance techniques. These methods approach the enthalpy as an average quantity over the entire flow field. However, it is known that the enthalpy varies significantly over the radius of the flow in an arc jet due to the way the gas is heated in an arc and due to wall cooling. Centerline measurements of stagnation point heat flux and pressure used in combination with a heat flux prediction correlation

---

<sup>1</sup> Insert Job Title, Department Name, Address/Mail Stop, and AIAA Member Grade for first author.

<sup>2</sup> Insert Job Title, Department Name, Address/Mail Stop, and AIAA Member Grade for second author

<sup>3</sup> Insert Job Title, Department Name, Address/Mail Stop, and AIAA Member Grade for third author

<sup>4</sup> Insert Job Title, Department Name, Address/Mail Stop, and AIAA Member Grade for fourth author.

<sup>5</sup> Insert Job Title, Department Name, Address/Mail Stop, and AIAA Member Grade for fifth author

<sup>6</sup> Consultant, 492 Enchanted Oak, New Braunfels, TX 78132, Associate Fellow AIAA

<sup>7</sup> Senior Research Scientist, Aerothermodynamics Branch, MS 230-2, Associate Fellow AIAA.

<sup>8</sup> Insert Job Title, Department Name, Address/Mail Stop, and AIAA Member Grade for eighth author.

or theory have been used to estimate the enthalpy of the flow in the center of the flow. One such correlation commonly used is one by Hiester and Clark<sup>1</sup> that is based on Fay and Riddell theory. Reference 1 compares the enthalpy derived by this formula with enthalpies determined in various ways for numerous facilities extant at the time. The correlation is not particularly good; nevertheless, it has been used extensively. A better way of determining local enthalpy of arc jet flows has been a goal of engineers for many years. Spectroscopic techniques, various laser scattering techniques, energy balance probes, and laser induced fluorescence (LIF) have been tried. An early survey was published earlier describing a number of the techniques.<sup>2</sup> Early measurements using copper LIF to measure the flow velocity were reported by Arepalli, et al.<sup>3</sup> Spectroscopy The LIF technique has been demonstrated to have the capability of obtaining almost all the parameters of the flow needed to determine the enthalpy when Bamford, et al.<sup>4</sup> used O-atom and N-atom LIF to determine flow properties; then later Fletcher<sup>5</sup> demonstrated the method for obtaining total enthalpy in pure nitrogen arc jet flow. Grinstead, Driver and Raiche<sup>6</sup> extended LIF measurements to determine radial distributions of various properties of nitrogen flow, but did not obtain enthalpy profiles. The LIF technique used is based on that of Niemi, et al.<sup>7</sup> as implemented by Grinstead, et al.<sup>3</sup> at the Ames Research Center. More recently, Lohle, et al.<sup>8</sup> used oxygen LIF to measure flow properties, including the enthalpy, in a pure oxygen plasma.

The present technique uses a laser for two-photon ultraviolet excitation of oxygen and nitrogen atoms to excited states that then radiate at infrared/visible wavelengths which are detected by a photomultiplier tube. The laser is scanned over wavelengths to obtain the spectral profile that consists of information about the temperature and velocity, plus its intensity is proportional to the atom density. With the calibration obtained using the technique of Niemi, et al.<sup>7</sup> one can obtain the atom densities. Because the excitation wavelength for nitrogen and oxygen are different, one must do the measurements with different configurations of the dye laser used to excited the atoms of oxygen and nitrogen. Sets of runs were made with two dye configurations, one for nitrogen and one for oxygen. This report documents the results obtained from the LIF measurements at the centerline of the arc jet flow, eight inches downstream of the nozzle exit. The present paper uses two-photon laser induced fluorescence of nitrogen and oxygen atoms, along with stagnation pressure measurements to determine the centerline enthalpy of arc jet flow at several operating conditions. Relative enthalpy distributions across the flow are estimated from relative stagnation heat flux and pressure distributions measured across the flow. The average enthalpy is determined from the centerline enthalpy and the radial distribution, under the assumption of a constant mass flux distribution. The accuracy of this assumption was assessed using a mass flux distribution calculated using computational fluid dynamics.

## II. The Experiment

### A. The Arc Jet Facility

This test program utilized test position 2 (TP2) which consisted of a ten-pack dual-diameter constricted arc column attached to a 15° half-angle conical nozzle with an exit plane diameter of 5 inches. A tungsten button cathode was used as the upstream electrode of the arc heater, and a conical copper anode is used as the downstream electrode. The arc heater contains 200 individually water-cooled, electrically isolated constrictor segments assembled in modular packs, 20 segments in each pack. The arc heated gas consisting of oxygen and nitrogen added to the flow separately. Nitrogen is injected at the cathode to avoid its oxidation. Oxygen is injected at various locations in the arc column. Gas is heated by a DC arc powered by a silicon-controlled rectified current of up to 10Mw.

### B. Laser System and Laboratory Optical Configuration

A simplified scheme of the experimental set-up is depicted in Figure 3. A tunable 30 Hz Nd:YAG (Continuum Powerlite Precision 9030) pumped dye laser (Continuum ND6000) provides visible radiation from 612 nm to 690 nm. The output of the dye laser is frequency-tripled using two auto-tracking  $\beta$ -barium-borate ( "BBO") crystal assemblies (Inrad AT-III) resulting in  $\sim 5$ ns pulses of vertically polarized coherent ultraviolet light between 204 nm and 230 nm with a pulse energy up to 4 mJ and a spectral bandwidth of approximately 0.25 cm<sup>-1</sup>. A four-prism harmonic separator is employed to separate the third harmonic laser beam from the dye laser fundamental and second harmonic laser beams. The two BBO crystals are automatically angle tuned using active feedback circuitry to provide constant output energy while scanning the dye laser wavelength. Two different laser dyes (Exciton) are used to achieve the desired atomic excitation wavelengths. To access the atomic nitrogen transitions, Rhodamine 640 perchlorate dye is used, while LDS 698 is used to access the atomic oxygen transitions. Approximately 20% of

the UV laser beam pulse energy is reserved for frequency and laser induced fluorescence (LIF) calibration measurements in the laboratory flow reactor. A pyroelectric energy sensor monitors the pulse energy directed through the flow reactor. The remaining 80% is directed out of the laboratory to the arc jet test cabin using a Class I fully enclosed laser beam transmission path.

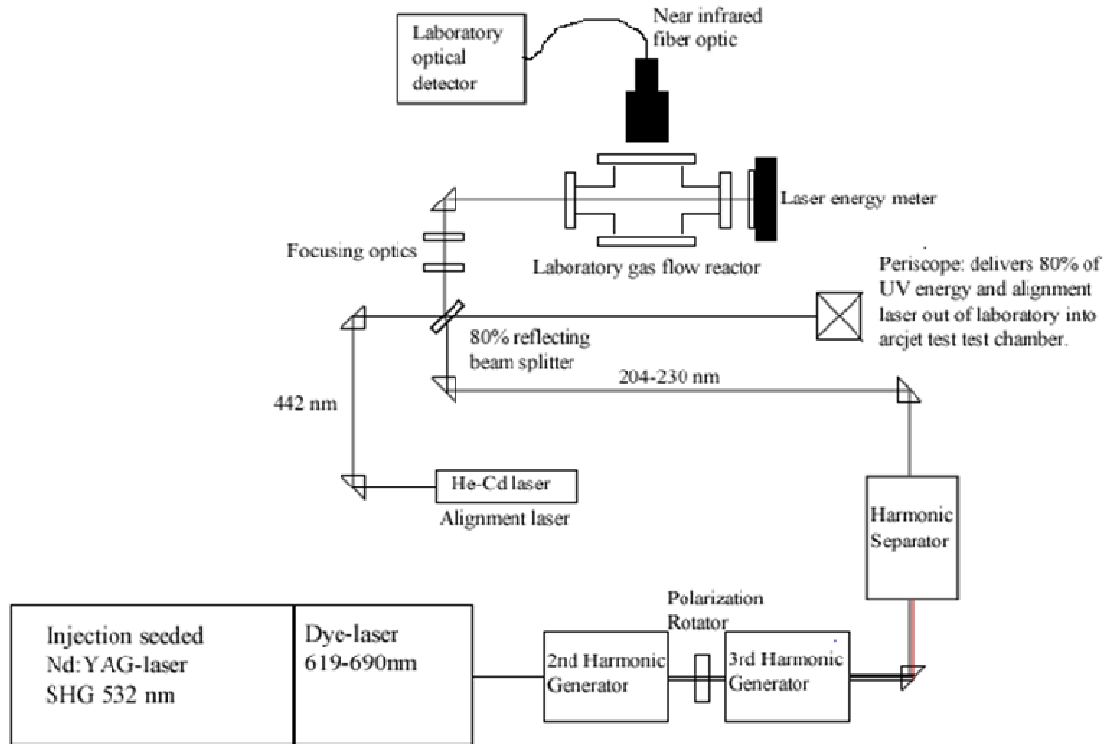


**Figure 1 Schematic diagram of the laboratory laser and optical configuration.**

### C. Arc Jet Optical Configuration

The optical configuration for the JSC test position #2 (TP2) was designed to enable single point LIF measurements on the flow centerline at prescribed locations from approximately 8 cm to 20 cm downstream of the nozzle exit. The portion of the laser beam to be transmitted to TP2 is elevated to approximately 2.5 m above the laser table, passes through an aperture in the laboratory wall, and is directed by a periscope (composed of right angle prisms) attached to a hatch on the side of the chamber. The beam enters TP2 through a dedicated fused-silica window. Mounted on the inside wall TP2 is an enclosed telescope that focuses the laser beam after it passes through the window. A four inch aluminum mirror directs the laser beam upstream to intersect the nozzle axis at a prescribed distance downstream of the nozzle exit. The entire beam transmission path from the optical table in the laboratory to the measurement location along the nozzle axis exceeds 10 m. Attachment points of periscope hardware to the facility enclosure were designed to minimize beam deflection due to thermal and vibrational stresses. As the overlap of the focused beam path with the region imaged by the collection optics is critical for repeatable absolute LIF intensity measurements, remotely controlled actuators operated from the laboratory are used to correct misalignment caused by cabin wall deflections or thermal drifts of the optics.

With the exception of the final element, all turning elements along the transmission path are fused silica right angle prisms with ultraviolet anti-reflection coatings (198 nm – 248 nm). The use of anti-reflection coated prisms rather than dielectric mirrors permits operation over the wavelength range required to access N, O, Kr, and Xe LIF without changing optics. The last turning element, which directs the beam into the flow at the non-normal angle necessary to realize a Doppler shift of the absorption profile, is a first surface, protected aluminum mirror with high (> 90%) reflectivity in the tuning range of the laser. The focused beam diameter at the measurement location is approximately 0.5 mm. A continuous-wave, frequency-doubled Nd:YAG alignment laser is coupled on to the transmission beam path. This laser is used for alignment purposes prior to testing.

The excited fluorescence is imaged from the probe volume and directed through a 1.37-inch clear aperture window located on the front face of TP2 at the 12 o'clock position directly above the arc heater column. The primary objective optic is a 3-inch diameter lens attached to a modified ring adapter plate that secures to the nozzle adapter plate within TP2. A four-inch protected gold surface mirror directs the imaged fluorescence horizontally to the integrated optical receiver which is located directly outside the vacuum chamber (TP2).

The LIF optical detector includes an alignment laser to enable proper alignment of the mounted mirror, primary objective, and receiver to the location of the probe volume. A motorized flip mirror, mounted inside the receiver, is used to intercept the collection optics path and couple a visible wavelength (red-diode laser) alignment laser on the path to back-illuminate the probe volume. The motorized flip mirror is remotely operated from the laboratory. The mirror also serves as an optical shutter to block the receiver photodetector when LIF measurements are not being performed.

#### **D. Titration**

To obtain the reference density of atoms in the flow reactor nitric oxide is added to the flow stream of nitrogen downstream of the discharge. It is added in such a way that good mixing is assured, via a multi-holed outlet vent inside the flow tube. The NO is added incrementally as the nitrogen atom LIF signal is measured. The point where the NO signal is extinguished (as determined by extrapolation) yields the amount of nitrogen atoms in the flow, which corresponds to the amount of NO that was introduced. In the present measurements this was  $8.48 \times 10^{13} \text{ cm}^{-3}$ . Under normal circumstances this would be the amount of oxygen atoms in the flow when oxygen is produced by reacting NO with N. However, there was a problem with the NO regulator that resulted in variations in the flow, hence the O-atom density.

#### **E. Data Acquisition**

An integrated LabVIEW and MATLAB software data acquisition remotely operates all subsystems of the experiment and records LIF data. The total LIF signal magnitude and fluorescence lifetime can be extracted from the time-resolved fluorescence pulse; therefore, a four-channel, 500 MHz digital oscilloscope (Tektronix TDS 5104B) was chosen to record the time-resolved fluorescence signals at each wavelength. The digital oscilloscope currently averages 8 fluorescence pulses at each step – with a wavelength step size of 0.002 nm – as the laser is scanned over the absorption features in the laboratory flow reactor and the arc jet. The MATLAB data acquisition system records all LabVIEW data and digitizes the waveforms collected by the oscilloscope. For each set of LIF data acquired, all relevant variables and waveforms are stored in a data structure within a MATLAB binary data file.

#### **F. Heat Flux and Pressure Probe Measurements**

The Heat Flux and Pressure Probe system consists of a chamber mounting assembly, a horizontal/vertical alignment plate, two 15-inch travel Velmex™ linear positioners, motion control and sensing hardware and software, and the water-cooled probe. Figure 3 shows the heat flux probe on the motion system as installed into the Test Position 2 (TP2) test chamber. The heat rate probe used for this test series is a Medtherm stagnation point heat flux probe, P/N 24-3000-18-72-21074, with a Gardon gage style heat rate sensor and a range of 0 - 3000 BTU/(ft<sup>2</sup>-sec). The probe assembly is made of OFHC Copper CDA 101 and is cooled with 500 psig de-ionized water. The probe tip at the sensor location is hemispherical with a 0.188-inch radius; and this hemispherical tip is located at the end of an approximately 1.75-inch length of 0.375-inch diameter copper tubing. (See Figure 4 which is an extract from the Medtherm drawing). The sensor is provided with a NIST-traceable calibration curve in terms of absorbed heat flux. The calibration curve is produced by extrapolating the data beyond the limit of blackbody reference sources (approximately an order of magnitude below the 3000 BTU/ft<sup>2</sup>-s upper limit) and by designing the sensor so that it will not be compromised at the upper limit. The water-cooled pressure probe has similar dimensions, but has an internal tube leading to a pressure transducer.



**Figure 2 Heat Flux Probe on the Motion System**

Vertical and horizontal alignment of the probes to the arc jet nozzle exit plane is facilitated using a laser to find the nozzle exit center, and a laser level to check for the trueness of the horizontal/vertical sweep across the length of the axis movement. The motion system uses a 5 V DC voltage supply and two string potentiometers to track the horizontal and vertical movement of the attached probe. Data signals from the position potentiometers are translated to positional data utilizing calibration curves input to the Test Data Acquisition System (TDACS). The accuracy of the potentiometer(s) are 0.25% of full scale, and the repeatability of the potentiometer output for a given position is 0.05% of full scale. The 5.0 VDC voltage to the potentiometers are supplied by two -10 to +10 VDC outputs from two 16-bit Digital to Analog (D/A) outputs; producing voltage output accuracy of  $\pm 3.512\text{mV}$ , or 0.07%. These accuracies produce a position reporting error of less than 0.01 inch. The individual linear axes are capable of movement accuracy of 1/400 (0.0025) inch increments, at feed rates of between 0.00025 in/sec to 1.5 in/sec.

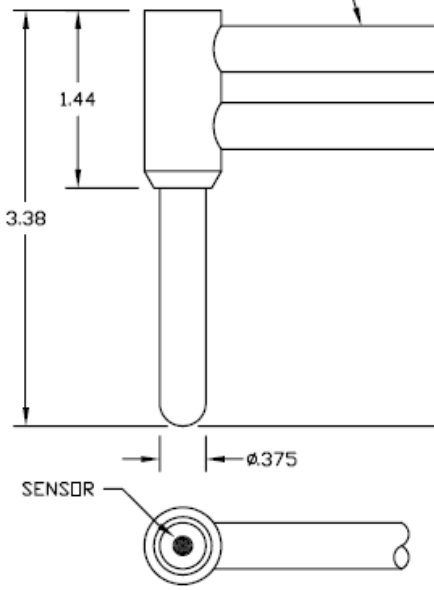


**Figure 3 Heat flux probe configuration with dimensions in inches**

### III. Analysis

#### G. Two Photon Laser Induced Fluorescence

##### 1. Calibration and reference atom source

The LIF signal measured by the PMT detector is given by

$$S(\nu_L, t) = f \left( L \frac{\Delta\Omega}{4\pi} \right) n \Phi \sigma_{12}^{(2)} \eta \varphi(\nu_L - \nu_o) \left( \frac{\varepsilon_p}{h\nu_L} \right)^2 \iint I_o^2 dt dA \quad (1)$$

Where  $f$  is the photomultiplier detector sensitivity in say, output volts per photon;  $\nu_L$  is the laser frequency; the laser energy squared is  $\varepsilon_p^2$ ; the collection volume  $L\Delta\Omega/4\pi$  seen by the detector; the atom density  $n$ , the quantum yield  $\Phi = \tau_{\text{obs}} / \tau_n$ , the ratio of observed to natural lifetime of the upper state; the two-photon excitation cross section  $\sigma_{12}^{(2)}$ ;  $\eta$  is the detector optical path transmission factor assumed to be constant over the laser scan wavelengths, including the filters;  $\varphi(\nu_L - \nu_o)$  is the normalized excitation line shape function; and the double integral term is the laser intensity distribution integrated in time and cross sectional space, which for conciseness shall be referred to as  $K_L$ . By integrating over time and frequency, we can simplify the notation by grouping various factors in Eqn. (1).

$$I = \eta K_G K_S K_L \left( \frac{\varepsilon_p}{h\nu_L} \right)^2 \Phi n \quad (2)$$

where

$$K_G = f L \frac{\Delta\Omega}{4\pi}$$

contains all the information about the collection volume, optical transmission, and detector efficiency;

and

$$K_S = \frac{\sigma_{12}^{(2)}}{(h\nu_L)^2}$$

contains information about the optical absorption transition.  $K_L$  contains the laser excitation information.

To calibrate the system as described earlier, the flow reactor provides a known source of atoms. They can either be a known species such as krypton or xenon at known temperature and pressure, or it can be the species to be measured in the arc jet, nitrogen or oxygen. Krypton has a fluorescence resonance at a wavelength very close to that of nitrogen; and xenon has a resonance wavelength very close to that of oxygen. We can therefore use these gases as calibration species to determine ratio of  $K_G$  in the arc chamber and the flow reactor. This is accomplished by placing a gas calibration cell at the location in the arc jet chamber where actual measurements will be made. This assures that the collection geometry is virtually identical in the calibration and in the actual arc jet measurement. The gas calibration cell and the flow reactor are set to known conditions of pressure and temperature; therefore, the density is known in both. The laser energy at both the flow reactor and the calibration cell are measured for each set of data, thus the dependence on laser energy can be included as the  $K_L$  factors. Neutral density and spectral filters for both are known. The spectra filters are the same for both the flow reactor and the fluorescence detector.

$$\frac{K_G^a}{K_G^r} = \frac{I^a K_S^r K_L^r \eta^r n^r \varepsilon^r}{I^r K_S^a K_L^a \eta^a n^a \varepsilon^a} \quad (3)$$

Since the laser characteristics and gases during calibration are the same (same wavelength and pulse profile) the  $K_S$  factors are the same, and the densities are the same (or can be taken into account) the geometry and detector efficiency ratios can be determined. Because of the proximity of the wavelengths of the calibration media (xenon or krypton) and their corresponding species to be measured, this ratio applies to both corresponding gases.

Then

$$\frac{K_G^a}{K_G^r} = \frac{I^a \eta^r \varepsilon^r}{I^r \eta^a \varepsilon^a} \quad (4)$$

All factors are known or measured quantities.

To determine the density of the unknown atoms in the arc flow a reference signal obtained in the flow reactor is used. A titration with NO provides knowledge of the atom density in the flow reactor. We can find the ratio of LIF response in the arc jet and in the flow reactor as

$$\frac{n^a}{n^r} = \frac{I^a \eta^r \varepsilon^r K_G^r}{I^r \eta^a \varepsilon^a K_G^a} \quad (5)$$

where the factors  $K_S$  and  $K_L$  for the flow reactor and the arc chamber, respectively, have divided out. All the quantities in this equation are measured or known.

## H. LIF Measurements of Arc Jet Flow

The laser was aligned to cross the arc jet axis at eight inches from the nozzle exit and a calibration cell containing xenon or krypton was installed at the central location. The fluorescence from this signal was used as reference for calibrating the system at a known temperature and pressure (density). The laser was scanned over wavelength and the LIF response was measured as a function of time at each wavelength. There were 500 time points recorded for each wavelength. The LIF signals were obtained as averages of eight laser pulses, with the laser pulse energy also recorded. However, the pulse energy signals were not synchronous with the LIF signals, therefore, an average of the laser energy for the scan was used for normalization. In the future, it is expected that a synchronous signal can be obtained so that each laser pulse, or average of the eight pulses can be normalized with its respective synchronous laser pulse energy. An average background versus time was determined from the first few pulses in the wavelength scan. The background was subtracted from the signal to obtain a relatively clean base. The background-subtracted LIF signals were integrated in time to yield spectral profiles. These spectral profiles were fit to Gaussian functions to obtain the central wavelength, amplitude, and width of the LIF signals. The nitrogen excitation spectrum has only one component, whereas the oxygen spectrum consists of three components. Relative strengths of the three components and their line positions were taken from Saxon and Eichler.<sup>9</sup> The raw data were also integrated with respect to wavelength to obtain the average time response for each wavelength scan. The time response data was fit to a Gaussian-exponential function that represents the convolution of the laser time pulse width and the LIF signal decay due to the natural decay and any quenching. Samples of the signals and the curve fits are shown in Figures 4

and 5 for spectra and time, respectively. The curve fit in time yields the decay constant, the amplitude of the fluorescent signal, and the laser pulse width.

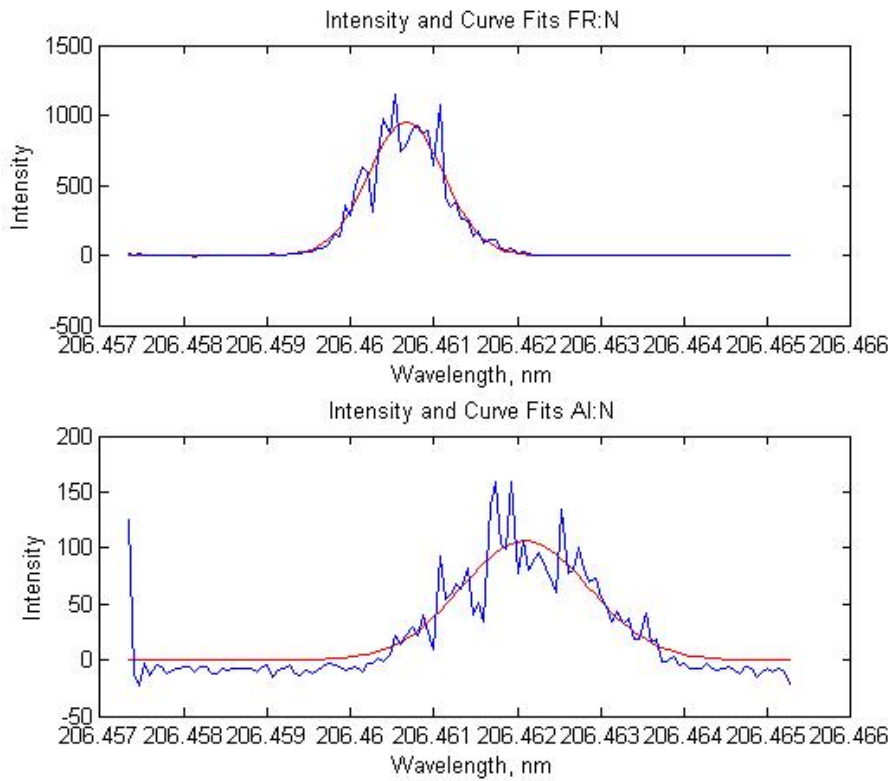


**Figure 4 Spectral data for sample laser scan of nitrogen atoms in the flow reactor and in the arc jet.**

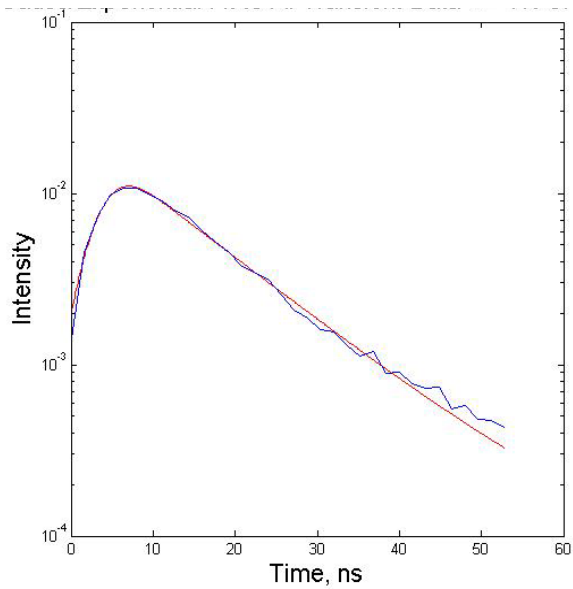


**Figure 5 Gaussian/Exponential fit to transient nitrogen LIF response in the arc jet.**

## IV. Results and Discussion

### I. Centerline Velocity and Temperature

From the relative central wavelength difference we obtained the flow velocity, taking into account the angle  $\theta=64.5^\circ$  of the laser beam with respect to the center line of the arc jet flow.

$$v = \frac{c\Delta\lambda}{\lambda_0 \cos\theta} \quad (6)$$

The velocities as function of arc current for various arc jet gas flow rates are shown in Figure 6.

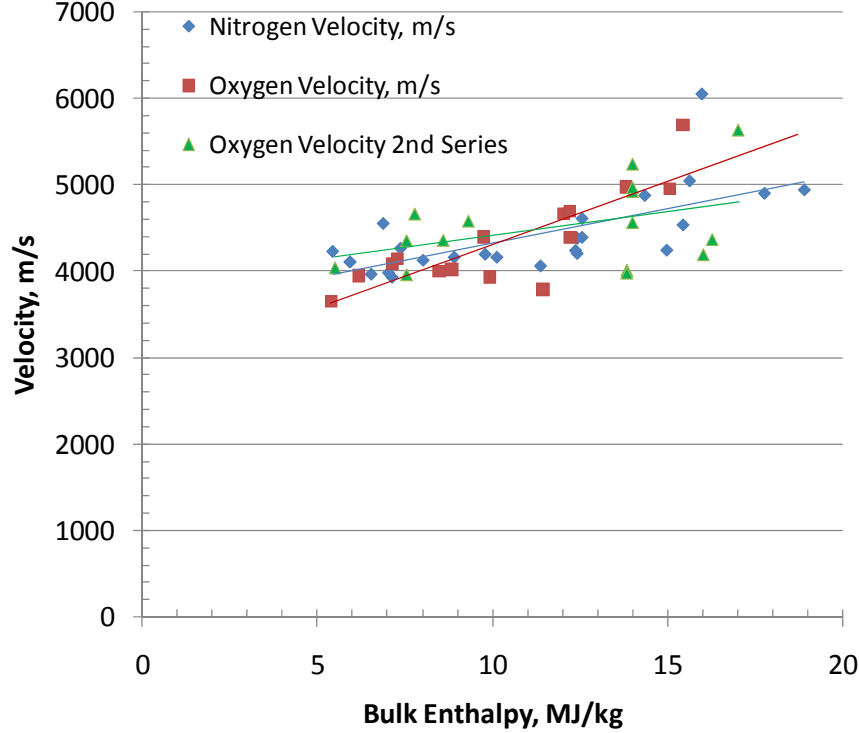


Figure 6 Velocities determined from Doppler shift of LIF spectral scans of nitrogen and oxygen

The temperature was estimated from the spectral widths using the standard Doppler Gaussian formula,<sup>5</sup> which takes into account the laser line width.

$$T = \frac{mc^2}{8 \ln(2)kn_A\lambda_0^2} [\Delta\lambda_{T,a}^2 - (\Delta\lambda_{T,r}^2 - \Delta\lambda_{D,r}^2)] \quad (7)$$

where  $\lambda_0$  is the central wavelength,  $\Delta\lambda_{T,a}^2$  is the full width at half maximum of the LIF signal in the arc jet,  $\Delta\lambda_{T,r}^2$  is the full width at half maximum of the flow reactor signal, and  $\Delta\lambda_{D,r}^2$  is the Doppler full width at half maximum at the flow reactor temperature. The terms in parentheses is the net laser line width squared. The flow reactor temperature was about 300 K. The temperatures are plotted versus arc current for various arc jet flow rates in Figure 7. It appears that the uncertainty in the temperature measurements dominate the results because we do not see a definite trend of temperature with arc current. One expects to see the temperature increase, as least somewhat, with arc current at a given gas flow rate.



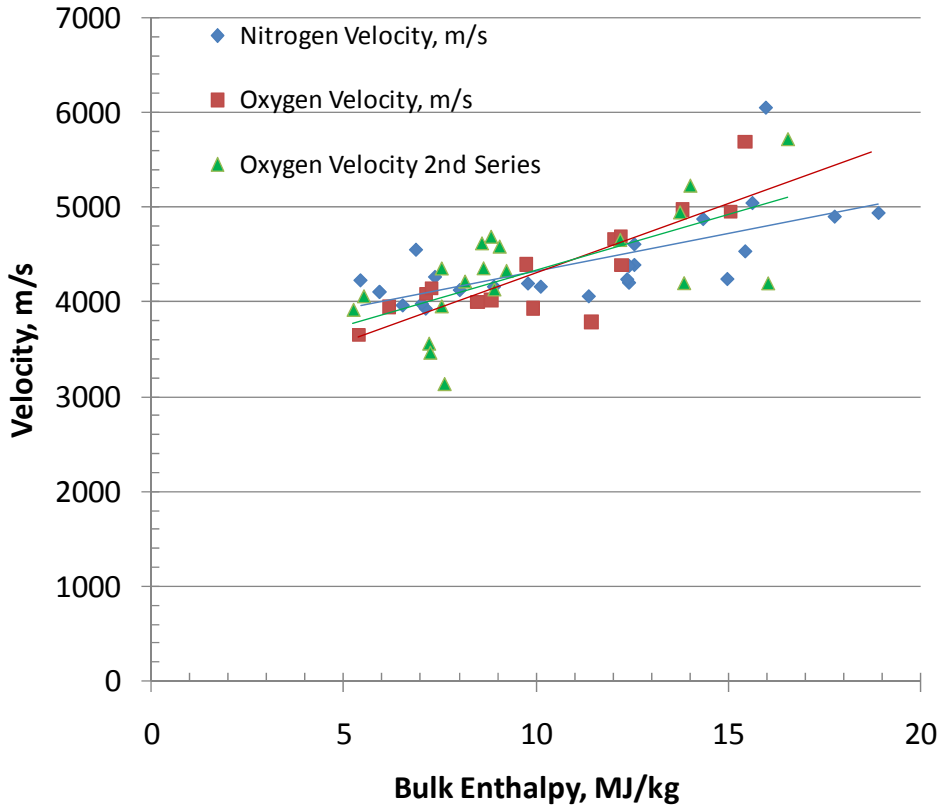


**Figure 8 Correlation of velocities with bulk enthalpy**

Enthalpy data from LIF measurements were only available where the stagnation point pressure is known for that case. The total enthalpy was determined by summing the components in each energy mode: kinetic, chemical, and thermal. The relation can be expressed as:

$$h_T = \frac{1}{2}v^2 + Y_N h_N^f + Y_O h_O^f + (C_{p_N} + C_{p_O} + C_{p_{N_2}} + C_{p_{O_2}})T \quad (8)$$

where  $v$  is the velocity measured by LIF,  $Y_N$  is the mass fraction of nitrogen measured by LIF,  $Y_O=0.23$  assuming all oxygen is dissociated,  $C_{p_i}$  are the specific heats for fully excited molecules  $C_{p/R} = 5/2$  for atoms and  $C_{p/R} = 7/2$  for molecules. The temperature was found by LIF measurements. The mass fractions were determined from nitrogen and oxygen number densities measured by LIF, and the density found from the hypersonic Pitot formula<sup>10</sup>

$$\rho \cong 2P_{t2}v^2/C_{pr} \quad (9)$$

where  $P_{t2}$  was the measured stagnation point pressure, and the hypersonic pressure coefficient is

$$C_{pr} = \left[ \frac{(\gamma+1)^2}{4\gamma} \right]^{\frac{\gamma}{\gamma+1}} \left[ \frac{4}{\gamma+1} \right] \quad (10)$$

The ratio of specific heats  $\gamma$  was assumed to be 1.5 for partially dissociated frozen flow. One method commonly used for determining local enthalpy of the flow is to use the formula from Hiester and Clark,<sup>1</sup> which they based on the Fay and Riddell stagnation point heating formula, assuming the Lewis Number = 1 and  $Pr=0.72$

$$h = 24.0q\sqrt{\frac{R_{eff}}{P_{T2}}} \quad (11)$$

where  $h$  is the total enthalpy in Btu/lb,  $q$  is the measured stagnation point heat flux in Btu/ft<sup>2</sup>/s,  $R_{eff}$  is the effective radius of the calibration model in feet, and  $P_{T2}$  is the measured stagnation point pressure in atmospheres.

### J. Enthalpy Distributions Based on Heat Flux and Pressure Probe Measurements

Heat flux and pressure distributions were measured at a distance from the nozzle exit of 2.8 inches. This is not the same as the eight inches from the nozzle that the LIF beam was focused on. However, since enthalpy is conserved along the centerline of the jet the enthalpy should not vary from one distance to the other.

Because both probes could not be installed at the same time in the chamber, runs were made with one probe; and then runs were made with the other probe at corresponding run conditions of arc current and flow rate. Initially, the probes were scanned stepwise, but it was determined that a continuous scan would be reasonable. This was especially true of the heat flux measurements since the Gardon gage sensor responded very quickly. The pressure measurements did not respond as quickly due to the volume of the sensing tube; therefore, it was necessary to scan more slowly. To enhance accuracy a scan in the positive direction was averaged with a scan in the negative direction with a weight function designed to bias the result toward the true value in the low pressure wings of the pressure distributions. Since the measurements were not at exactly the same  $y$ -distance from the axis, the heat flux distribution and the pressure distribution were interpolated at a set of common  $y$ -distances. The pressure distribution for an example case is shown in Fig. 9. Then, equation (11) was applied to determine an estimate of the local enthalpy at each  $y$ -distance. An example of the heat flux and pressure distributions and the resulting enthalpy distribution is given in Fig. 10.

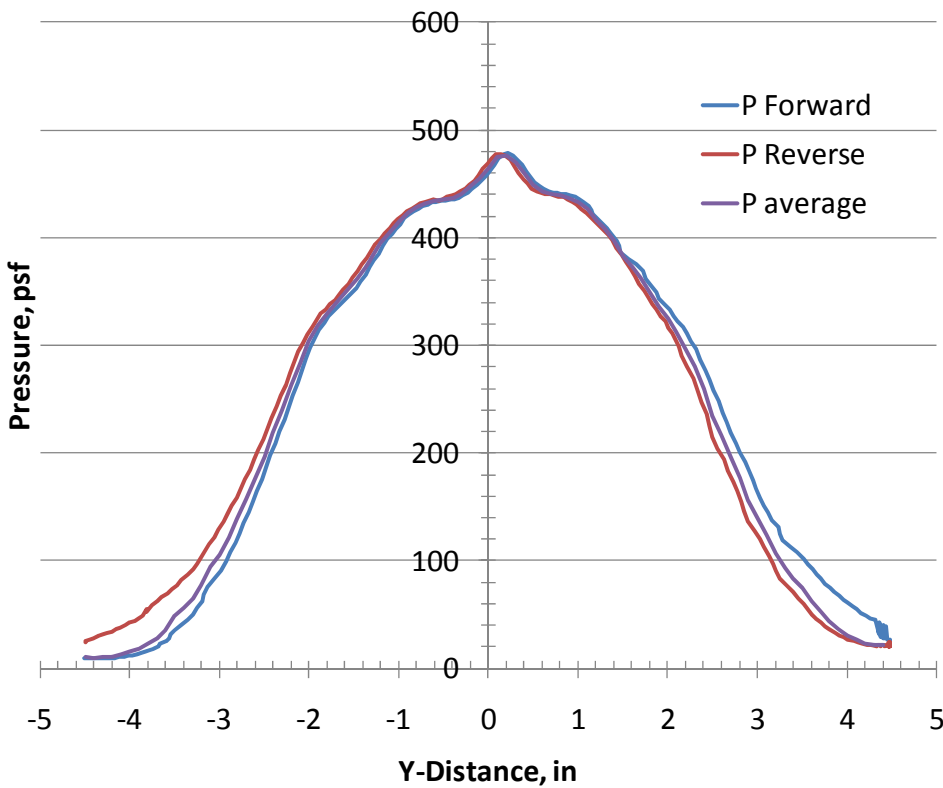
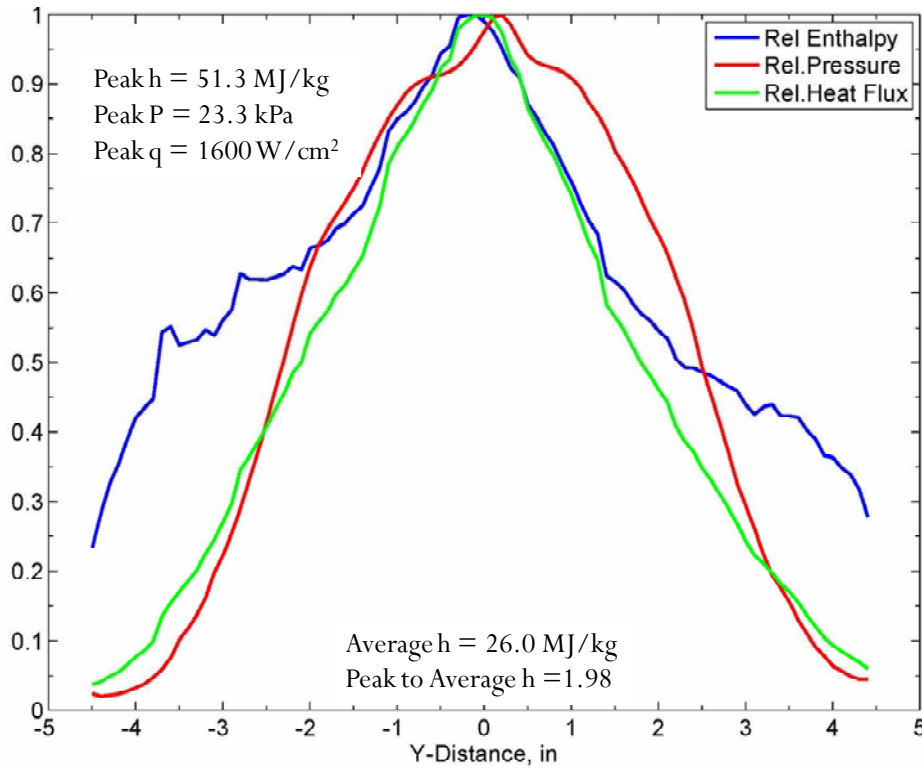


Figure 9 Measured pressure sweep in the positive and negative directions with the weighted average distribution 0.25 lb/s and 1200 A.



**Figure 10 Relative distributions of heat flux and pressure measured at a flow rate of 0.25 lb/s and arc current of 1200 A with the corresponding enthalpy distribution.**

The distributions were normalized with the central point and the positive and negative point were averaged to obtain a radial distribution of the enthalpy. The radial distribution was averaged over the radius of the flow (taken to be 5 inches) to find the average enthalpy using the relation

$$h_{ave} = \frac{2\pi \int_0^R r m(r) h(r) dr}{2\pi \int_0^R r m(r) dr} \quad (12)$$

where  $m(r)$  is the relative mass flux distribution and  $h(r)$  is the relative enthalpy distribution as functions of radius  $r$ . Initially, it was assumed that the mass flux was constant across the jet since we did not have a measure of the mass flux. However, to assess the potential error in the average enthalpy, we decided to use a mass flux distribution determined from computational fluid dynamics (CFD) calculations made previously for cases similar, but not the same at the test conditions of the present measurements. The mass flux distribution determined in this way is shown in Fig. 11. The same relative mass flux distribution was used for all determinations of the average enthalpy. Peak to average enthalpies for each test condition were computed from the distributions shown in Fig. 11. These ratios were then multiplied by the measured heat balance bulk enthalpy to obtain an estimate of the centerline enthalpy to be compared with the central value based on Eqn. (11). The results are shown in Fig. 13. Results of the LIF based calculations of total enthalpy and the enthalpy derived from stagnation point heat flux and pressure measurements are also shown in Figure 12. These values agree somewhat well at low arc currents, but the LIF measured point at 1800 amps appears too low in comparison. It can be seen that the probe centerline enthalpies and the compare favorably with the bulk enthalpy multiplied by the peak to average ratio. Better agreement is obtained when the CFD-derived mass flux distribution is used to determine the peak to average enthalpy ratio. There is quite a bit of scatter in the LIF-based enthalpy. This might be expected because of the many separate measurements that are involved in determining the enthalpy by this technique. However, the agreement is fairly good.

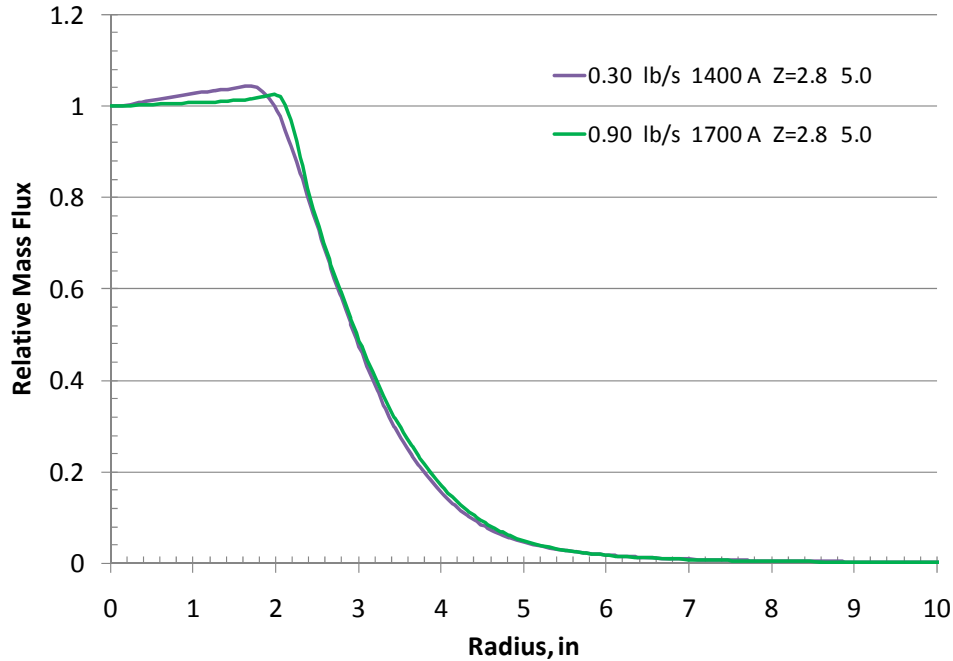


Figure 11 Mass flux distributions at two test conditions calculated by CFD (courtesy Maxim Larin). Distance from a 5-inch diameter nozzle is 2.8 inches.

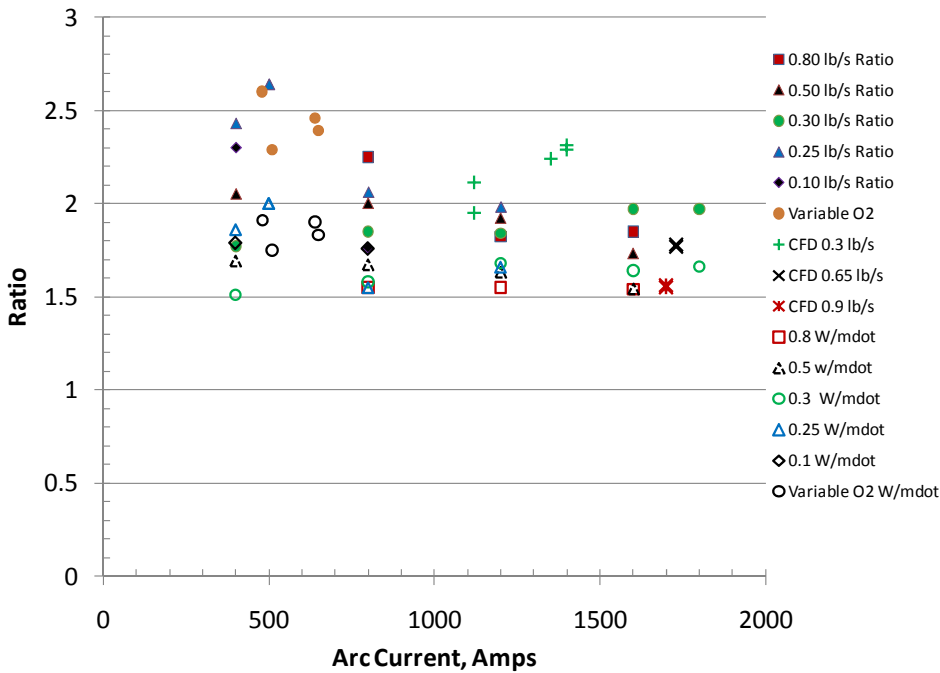
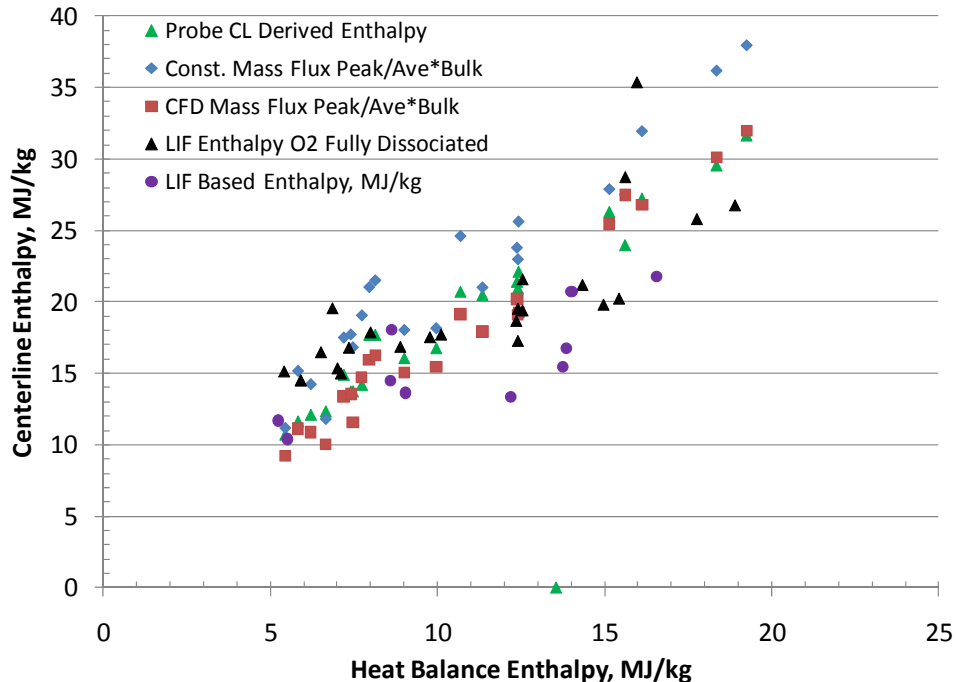


Figure 12 Summary of peak to average enthalpy determined assuming constant mass flux distribution and CFD-derived mass flux distribution.



**Figure 13 Comparison of centerline enthalpy derived from centerline heat flux and pressure probe measurements, from probe distributions assuming constant mass flux distribution and with CFD derived mass flux distributions, and from LIF measurements of flow properties. Also shown is the enthalpy based on nitrogen LIF that assumes full oxygen dissociation.**

## V. Conclusion

The decades old goal of determining the total enthalpy of arc jet flow has been realized with the use of probes and laser induced fluorescence. The comparison is rather good, but there is still many variables that can induce error into the LIF measurements. Having a good estimate of the centerline enthalpy will help thermal protection material analysts use obtain better estimates of the actual enthalpy obtained in materials tests. Since the bulk enthalpy as determined by energy balance measurements is always made in the arc jet of the Johnson Space Center facility, having the ratio of centerline to average enthalpy as determined by probe heat flux and pressure distributions will help expedite determining the centerline enthalpy of the test flowfield.

## Acknowledgments

The authors wish to acknowledge the contributions of Dr. Sivaram Arepalli and Mr. Chris Harris for their help in initiating the LIF work.

## References

- <sup>1</sup> Hiester, N. K. and Clark, C. F., "Feasibility of Standard Evaluation Procedures for Ablation Materials," NASA CR-379, February 1966.
- <sup>2</sup> Carl D. Scott, "Survey of Measurements of Flow Properties in ArcJets", *J. Thermophys. Heat Transfer* 7, 9 (1993).
- <sup>3</sup> S. Arepalli, E. H. Yuen, and C.D. Scott, "Application of Laser Induced Fluorescence for Flow Diagnostics in Arc Jets", AIAA 90-1763 (1990) .
- <sup>4</sup> Bamford, D., A. O'Keefe, D. Babikian, D. Stewart and A. Strawa. "Characterization of Arc-Jet Flows Using Laser-Induced Fluorescence." *AIAA Journal Thermophysics and Heat Transfer* 9 (1994): 26-33.
- <sup>5</sup> D.G. Fletcher, "Arcjet flow properties determined from laser-induced fluorescence of atomic nitrogen," *Applied Optics*, Vol. 38, No. 9, 20 March 1999, pp. 1850-1850.

---

<sup>6</sup> J.H. Grinstead, D.M. Driver, and G. A. Raiche, "Radial Profiles of Arcjet Flow Properties Measured with Laser-Induced Fluorescence of Atomic Nitrogen," in *Instrumentation in Aerospace Simulation Facilities*, 2003. ICIASF '03. 20th International Congress on, 25-29 Aug. 2003, pp. 278 - 286

<sup>7</sup> K. Niemi, V. Schulz-von der Gathen, and H. F. Döbele, "Absolute calibration of atomic density measurements by laser-induced fluorescence spectroscopy with two-photon excitation," *J. Phys. D. Appl. Phys.* **34** pp. 2330-2335 (2001)

<sup>8</sup> S. Löhle, C. Eichhorn, A. Steinbeck, S. Lein, G. Herdrich, H-P. Röser, and M. Auweter-Kurtz, "Oxygen plasma flow properties deduced from laser-induced fluorescence and probe measurements," *Applied Optics*, Vol. 47, Issue 11, pp. 1837-1845 (2008)

<sup>9</sup> R. P. Saxon and Jörg Eichler, "Theoretical calculation of two-photon absorption cross sections in atomic oxygen," *Phys. Rev. A*, Vol. **34** No. 1 July 1986, pp. 199-206

<sup>10</sup> J. D. Anderson, *Hypersonic and High Temperature Gas Dynamics*, McGraw-Hill Book Co., New York (1989)